NREL/SR-520-24760 • UC Category: 1262

Atomic-Scale Characterization of Hydrogenated Amorphous-Silicon Films and Devices

Annual Subcontract Report
15 April 1994 - 14 March 1998

A. Gallagher, S. Barzen, M. Childs, and A. Laracuente
National Institute of Standards and Technology
Boulder, Colorado

NREL technical monitor: B. von Roedern

National Renewable Energy Laboratory
1617 Cole Boulevard
Golden, Colorado 80401-3393
A national laboratory of
the U.S. Department of Energy
Managed by Midwest Research Institute
for the U.S. Department of Energy
under Contract No. DE-AC36-83CH10093

Prepared under Subcontract No. DAD-4-14084-01
June 1998

NOTICE

Available to DOE and DOE contractors from:
Office of Scientific and Technical Information (OSTI)
P.O. Box 62
Oak Ridge, TN 37831
Prices available by calling (423) 576-8401

Available to the public from:
National Technical Information Service (NTIS)
U.S. Department of Commerce
5285 Port Royal Road
Springfield VA 22161
(703) 487-4650

Printed on paper containing at least 50% wastepaper, including 20% postconsumer waste

Preface

This report describes the results from the period April 15, 1996 to March 14, 1998, carried out by the National Institute of Standards Technology (NIST) under contract DAD-4-14084-01 from the National Renewable Energy Laboratory. The results for the period of April 15, 1994 to April 14, 1996 are referenced below. The research is carried out under the direction of Dr. Alan Gallagher, a NIST physicist, in "JILA" on the University of Colorado campus in Boulder, Colo. Under a subcontract with the University of Colorado, graduate students and post-doctoral students of the University work on the project. During the period covered by this report the students have been: Stefan Barzen, a graduate student who carries out the scanning tunneling microscope measurements, Arnaldo Laracuente, who graduated in September, 1996, and post-doctoral student Michael Childs, who carries out the studies of discharge particulates.

Abstract

The research is concerned with improving the electronic properties of hydrogenated amorphous silicon (a-Si:H) films and of photovoltaic (PV) cells that use these films. Two approaches toward this goal are being taken. One is to establish the character of silicon particle growth in the rf glow discharges that are used to make the films and PV cells, and to understand the particle incorporation into the films. The ultimate goal of this effort is to find mitigation techniques that minimize the particle incorporation. During this contract period we have developed a novel particle light-scattering technique that provides a detailed and sensitive diagnostic of small (8-60 nm diameter) particles suspended in the discharge. We have used this to measure the particle growth rates and densities, versus conditions in pure-silane discharges. The second program is directed toward measuring the electronic properties of thin-film PV cells, as a function of depth within the cell. The approach being taken is to use a scanning tunneling microscope (STM) to measure the depth-dependent electronic properties of cross-sectioned PV cells. During the present period, measurements on single and tandem amorphous silicon cells have been carried out. Using STM current-voltage spectroscopy, these measurements distinguish the boundaries between the highly-conducting and intrinsic layers, as well as the chemical potential versus depth in the cell.

Summary

Goal

The first objective of this work is to establish methods that diminish the incorporation of Si particles into the films of a-Si:H PV cells. These particles are not large enough to induce shorts, but they are sufficiently numerous to have a major effect on electrical and structural quality. To achieve this objective we need to understand the growth and behavior of particles in the discharges currently used to deposit a-Si:H, PV cells, and why these particles incorporate into films during film growth. Using this understanding, we can devise and test methods of modifying the deposition techniques to diminish this particle incorporation.

A second part of the program is designed to measure the distributed electrical properties within PV cells. The purpose is to assist manufacturers in improving cell properties. By isolating junction regions or regions within the i-layer, versus illumination, light soaking and external biasing, we hope to improve understanding of where inefficiencies arise within the cells. The method employed is STM tunneling into cross-sectioned cells in a UHV environment, using the current-voltage behavior of the STM current to deduce the cell properties versus position through the exposed layers of the cell.

Results

In the present study of particle growth in the silane plasmas used to produce a-Si:H films, we developed a new light-scattering method that discerns particle size and density versus position in the discharge, for the very small particles that grow above the substrate. This method is sensitive to 8-60 nm diameter (ϕ) particles, and has allowed us to deduce particle growth above the substrate. In contrast, our previous method of pulsed-laser scattering and independent detection of the scattering from each particle was sensitive to ϕ>50 nm particles, which reside at the downstream end of the discharge for conditions used in device manufacturing. We have developed a model for this particle growth in the center of the discharge; this can explain some but not all of the particle growth results.

The other component of our research is designed to measure the properties of cross-sectioned PV cells with a STM. During this period this effort has achieved the primary goal of developing the tool and methodology to allow such measurements. We have used this to measure the STM current (I) voltage (V) relationship, with ~2 nm resolution, at each position across the cleaved surfaces of a single and a tandem-junction a-Si:H cell. This I-V relation is diagnosed to establish the boundaries between highly conducting and intrinsic regions, and an apparent (or chemical) potential is also established versus position in each cell.

TABLE OF CONTENTS

Introduction

Particulate growth in plasmas is ubiquitous, and is now widely recognized as a serious problem in almost all plasma processing, in etching as well as deposition discharges. Although the clear-cut effects of large (>0.3 μm) particles on circuits are apparent, much smaller particles are commonly incorporated into growing films, and these have more subtle effects on the film electrical properties. Silicon particulates readily form in a-Si:H deposition discharges, but they become negatively charged in the discharge and this is normally expected to trap them in the plasma and prevent their incorporation into the growing film. Thus, particles have primarily been expected to be a problem only when the discharge is switched off and they can reach a surface. However, we now know that very small particles can continuously incorporate into the film during growth, and with sufficient density to potentially be the primary cause of a-Si:H film inhomogeneities and electrical defects [Tanenbaum et al. 1995, Tanenbaum et al. 1996, Gallagher et al.1995]. There is every reason to expect poor Si-Si bonding at the particle-film interfaces, with deleterious effects on gap state densities. This is supported, but not proven, by measurements that have shown a dependence of film optical properties on the presence of particles in the discharge [Schmidt et al. 1993]. The basic cause of this continuous particle escape from the plasma is the modification of the plasma properties by very large densities of very small particles. When the particle charge density becomes comparable to the positive ion density, many particles become neutral and can reach the substrate, where they incorporate into the growing film. Thus, it has become quite important to establish the character of particle growth and trapping in a-Si:H deposition discharges, and ultimately to decrease their incorporation into a-Si:H, photovoltaic (PV) cells.

Light scattering is the most common method of detecting particles suspended in discharges, as it is non-obtrusive and can establish spatial distributions. But as normally applied it has serious limitations for the present problem of observing the very small particles, with diameter $\phi < 20$ nm, which are incorporated into the a-Si:H film. In small-particle light-scattering measurements, the scattered intensity is proportional to $N_p \phi^6$, where N_p is the particle density. Thus, the scattering signals are very small for these small D particles, and in addition it is necessary to establish either ϕ or N_p by an independent method. Our initial studies of particle behavior in these silane discharges, reported in our previous Annual Report [Gallagher et al. 1997], utilized a method of detecting pulsed-laser scattering from individual particles. We had hoped that this would be sufficiently sensitive to detect particles with $\phi \geq 10$ nm, but only $\phi \geq 30$ nm sensitivity was achieved because the particles evaporated in the intense laser beam. Although we could infer some important factors about particle growth in these discharges [Gallagher et al. 1997], this was not as useful as measuring the growth that occurs directly above the substrate. Thus, during the present contract period we developed and used a light-scattering method that is sensitive to smaller particles. This has allowed us to measure particle growth and density, directly within the discharge, for $\phi \geq 8$ nm. The results thereby obtained are presented below.

PV cells contain several layers and junctions, and it is quite difficult to independently establish the behavior of these different components and junctions in the composite structure. A variety of sophisticated optical and electrical measurements provide valuable hints regarding the locations and causes of cell efficiency losses, but unique connections to particular locations or junctions are not available. In this part of our program, we have been developing a measurement method that more uniquely separates the electrical behavior of each region of a PV cell. This is based on scanning tunneling microscope (STM) spectroscopy of cross-sectioned cells. The ultimate objective is to measure the shapes and positions of the bands and quasi Fermi levels, at all positions within an operating cell, using STM current-voltage spectroscopy at each location through the cell. However, the method of

measuring the band edges has not yet been established even for STM measurements on crystalline semiconductors, so we have so far concentrated on measuring an "apparent potential", which is closely related to the chemical potential and the quasi-Fermi levels. During this contract period we have solved many technical problems to obtain these measurements on a single junction and a tandem-junction a-Si:H cell. The resolution of these technical issues, as well as the character of the observations are presented below.

STM Measurements on Cross Sectioned PV Cells

As described in the Introduction, our intent is to cleave PV cells in ultra-high vacuum (UHV) and use a STM to measure the electrical properties of the operating cell at each location through its exposed cross section. We will first describe technical complications, which have occupied much of our efforts during this contract period. Many of the technical difficulties are now satisfactorily overcome, using the techniques described, but others are still being worked on.

The first issue is obtaining a relatively flat, cleanly cleaved cell surface that has not been exposed to air. For this reason, we have so far studied only cells on glass substrates. To make the cleave in vacuum, we diamond-scratch the back surface of the glass and partially strain-cleave it in air, using brief contact to a hot tungsten wire. Then, after transferring the sample to vacuum the glass surface is pushed to complete the cleave.

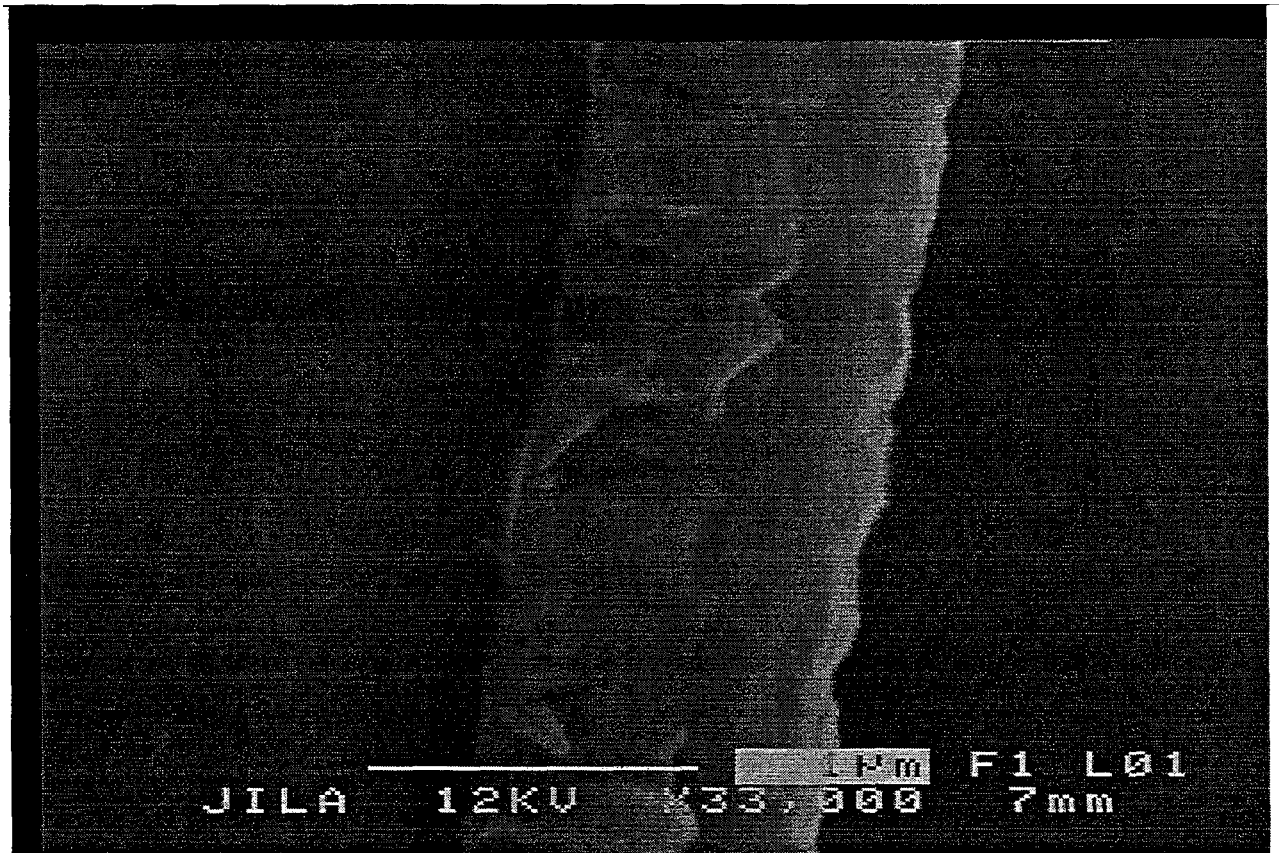

Fig: 1 Scanning Electron Microscopy image of the cleaved Solarex tandem cell.
The image was taken perpendicular to the cleaved surface, one sees the glass substrate on the left side, the textured SnO, the smoother a-Si:H tandem cell with a ZnO and Al contact layer on top. The dark right side is the background of the SEM chamber. The line at the bottom is 1 µm

A series of investigations with a Scanning Electron Microscopy (SEM) showed that the partial strain-cleave is absolutely essential to obtain clean cleaves without leaving big pieces of debris or tearing parts of the films off. A SEM picture of a cleaved surface, obtained with this cleaving method, is shown in **Fig.1**. So far two different a-Si:H cells have been investigated. The single cell, obtained from NREL,

has a metal layer directly on the a-Si:H, and this does not adhere well during the cleave. When we deposit a 5 nm Au-Pd layer on exposed sections of the a-Si:H, we obtain an acceptable metal-layer cleave. For this cell, which is deposited on smooth indium-tin-oxide (ITO), this provides a flat surface with a sharp corner at most locations along the length of the cleave. An interesting distinction has been observed with the STM and the SEM between the shapes of the cleaved a-Si:H and TCO surfaces (see Fig.1). The a-Si:H cleaves to an almost atomically flat surface, with typically <0.5 nm height variations out of the cleavage plane. In contrast, the cleaved ITO surface contains many hills of ~ 20 nm height and 40 nm diameter, that protrude above a relatively smooth cleavage plane. This is due to crystals imbedded in an amorphous network. The tandem cell, obtained from Solarex Corp., has an Al top layer on transparent conducting oxide (TCO), and we find that this Al layer is well adhered so that in most regions it cleaves at the edge of the TCO. This cell described below is deposited on highly structured TCO to enhance light trapping, and as might be expected this cleaves to yield a much rougher surface.

The next issue is to place the STM probe tip over the approximately 1 μm thick end of the cell without "crashing" it on the nonconducting glass surface. This is done using high quality, in-vacuum optics to position the probe within a few μm of the conducting side of the cell, near the cleaved end. A computer controlled approach then involves (1) translating the sample sideways until tunneling occurs between the corner of the cell and the side of the probe, followed by (2) a scan in tunneling to establish the slope of the sample-probe contact, and (3) backing up the sample by ~1 μm and repeating. In this manner the probe travels around the corner of the cell and never passes over the glass substrate. The overall sample-holder and probe arrangement is shown in **Fig.2**.

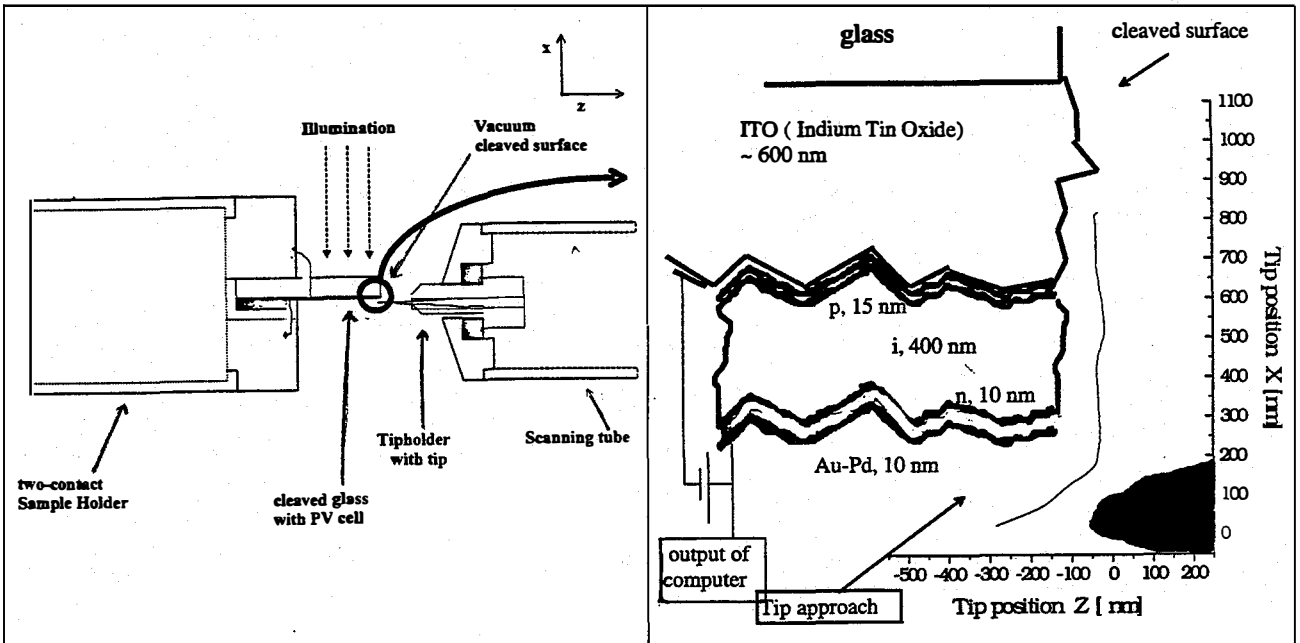

Fig: 2 a) Top view onto sample holder and STM
The solar cell is mounted into the two contact sample holder which can be moved by 'inchworms' and piezo actuator. A computer controlled combination of moving the holder and test scans of the tip maneuver the tip around the edge.

b) The curve shows the measured trace of the tip scanning 800nm across the edge and the NREL solar cell. The inserted drawing gives an idea of the size and location of the tip and the cell, which is externally biased in this case.

We can detect the moment when the STM probe reaches the cleaved surface by two observations. First, the slope of the scanned surface is greatly reduced compared to the traversal of the tapered probe around the corner of the sample. Next, we measure the apparent potential of the surface at each point, and this varies across a biased cell. This overall approach method often works, but the probe tip sometimes becomes "dirty" with atomic debris when rounding the corner. This causes unacceptably noisy tunneling over the exposed surfaces of the cell, TCO and contacts. We can sometimes adequately clean the probe in-situ with large (e.g. 20 V) voltage pulsing when tunneling above the ITO or metal. This leaves atomic debris on this part of the sample, so we then move to a new area, typically 100 nm away. If this is not successful, we must remove the probe from the STM for high temperature (~1500 C) cleaning in another part of the UHV chamber, then repeat the full approach process after the probe cools. For this reason, we have recently devoted considerable effort to improving the sample position manipulations, which are based on a combination of Burleigh "inchworms" and piezoelectric translators. Some components of these manipulators are shown in the last report [Gallagher et al. 1997].

Another issue is the passivation of the cleaved a-Si:H surface, as surface states could severely bend the bands near the surface. This is a primary concern for the intrinsic layers. To study this we sometimes expose the cleaved surface briefly to H atoms from a hot W filament, using ~10^{-4} Torr H_2 inside the UHV chamber. Since the exposed Si bonds within a-Si:H are H passivated, this should be an effective passivation procedure for these layers. We do not yet have sufficient data to establish clearly if this has an effect on the measurements. H atom bombardment may reduce the surface of the TCO layers. Any effect this has on the junction between the TCO and the doped a-Si:H can be established by comparison to the junction behavior before H exposure, but this has not been done yet. Another possible passivation treatment is exposure to an H_2 discharge; again this has not yet been tested.

We find that it is very important to have atomically clean probes and sample surfaces, and we now obtain these using chemically-assisted high-temperature sample and probe cleaning and annealing in UHV. (Most reported STM measurements are not made with atomically clean and metallic probe surfaces.) When this is done on a clean metallic surface with a clean probe we find that the tunneling resistance (R_t) reduces to <10^4 Ω with ~0.5 nm reduction of the tunneling gap. (If one attempts this with a W probe cleaned in the standard manner of most STM laboratories (heating to >1500 C in UHV), the WO_x layers on the probe surface form a barrier that prevents R_t from dropping bellow ~10^5 Ω.) When this same measurement method is performed on a TCO surface we find that the tunneling resistance only reduces to <10^6 Ω with ~0.5 nm reduction of the tunneling gap.

Two of the most serious issues are achieving meaningful STM current-voltage (I-V) characteristics at each position within the cell, and interpreting these. For this purpose, we initially studied I-V characteristics on p and n type crystalline Si and metal surfaces. With those clean probes we performed STM spectroscopy on the c-Si by ramping the voltage at defined tunnel distances with the feedback turned off. Examples of our results are shown in **Figs. 3& 4.** We believe these are state-of-the-art results, but unfortunately that does not mean they can be easily interpreted to yield band energies. We are currently investigating available models that are used to interpret such STM I-V spectroscopy, but those found so far appear to be inadequate for our purposes. The main reason is the drastic impact of surface states on the work function and band bending, as well as the influence of the high current density and the electric field in the tunneling gap. Thus, it is not yet clear if I-V data versus position in the cell can be used to obtain information on the positions of the band edges.

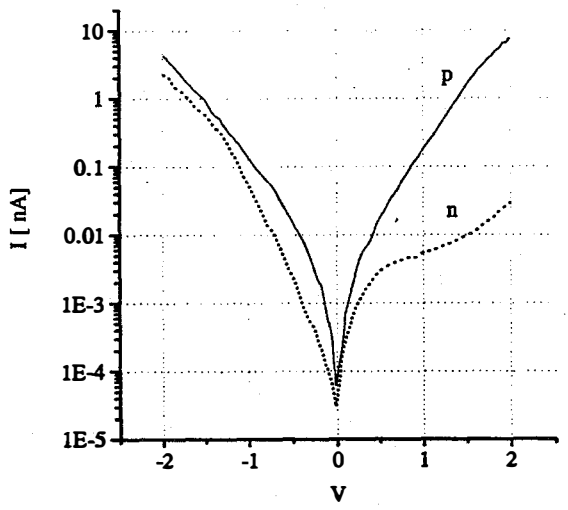

Fig: 3 STM I (current)-V (voltage) spectroscopy on H-passivated n and p type c-Si(100)

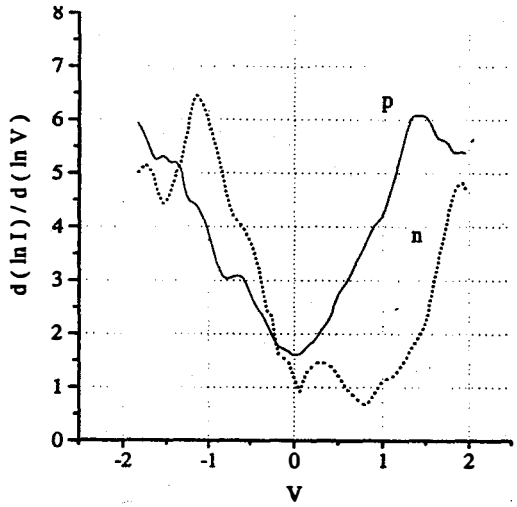

Fig: 4 In standard STM 'current-voltage-spectroscopy' the logarithmic derivation d (ln I) / d (ln V), shown here is assumed proportional to the semiconductor density of states (DOS). But the results vary with the tunnel gap and surface position.

Obtaining STM I-V characteristics on the intrinsic a-Si:H layer is the next and most difficult problem. Due to the low conductivity of the intrinsic layer, we must carry out I-V measurements at the lowest feasible currents to reduce local distortion of the bands. For this purpose we have developed a low current STM amplifier that can measure in the fA region.

Next, we have developed a computer-controlled operation that establishes the STM I-V characteristics, at each location across the cleaved cell, as a function of the probe-sample gap. This is carefully done in a manner that avoids "crashing" the probe into the cell surface and thereby covering the probe tip with debris. That readily occurs if one attempts to decrease the tunneling gap in feedback, by lowering the tunneling voltage. Therefore, we stop current feedback, move the probe a controlled distance (usually 0.3-1nm) forward from the tunneling condition, measure the I-V relation, retract the probe to the original position, and restore feedback at the standard condition (usually -2 V bias and 1 nA).

The next issue is to establish the locations of the various cell layers when moving the STM probe across the cell. We use differences in the I-V characteristics for this purpose. On a conducting layer like the TCO, the effective junction resistance continually decreases as the probe is moved closer to the cell, always reaching $<10^6\ \Omega$ at low voltage. The I-V relation is also overall symmetric and resistive, as is shown in **Fig. 5a** at the ZnO and in **Fig. 5e** above the SnO of the Solarex tandem cell. In contrast, as the probe is moved toward smaller tunneling gap on the intrinsic layer, the tunneling resistance saturates at a value $>>10^6\ \Omega$, even in contact, as seen in in **Fig. 5b** and **Fig. 5d** above the intrinsic layer of the top and the bottom cell respectively. In essence, a Shottky barrier is formed between the probe and semiconductor and an asymmetric I-V is then obtained, as occurs for Shottky junctions. **Fig. 5c** shows the I-V curves in the region of the p-n junction between the two cells.

The data in **Fig. 5** indicates that we can clearly distinguish between layers of the cell. Curves above the

ZnO/Al layer are sometimes noisier, probably due to debris, but otherwise on clean areas the spectroscopic I-V data are reproducible. Measurements on the single cell from NREL showed also the same type of I-V behavior, and the two contacts and the intrinsic layers were very distinct in their current-voltage dependence. However, in both cells it was hard to find a clear difference between the doped semiconductors and the close-by intrinsic areas. Probably the automated measurements of the conductivity at low voltages while scanning across the films will yield additional insights into this junction.

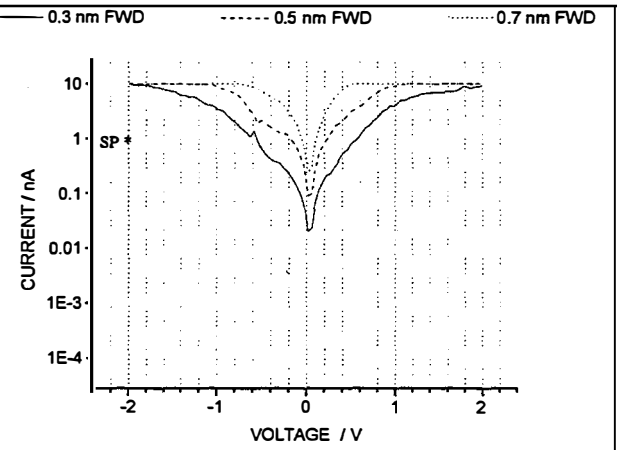

Fig. 5. I-V curves
a) I-V curves at 3 different tunnel gaps above the ZnO or Al layer. *SP marks the setpoint at 2 V and 1 nA. The films are highly conductive, the symmetry indicates a metal like density of states and the apparent potential V_a (the zero current point) is at 0 V, since this contact is the reference.

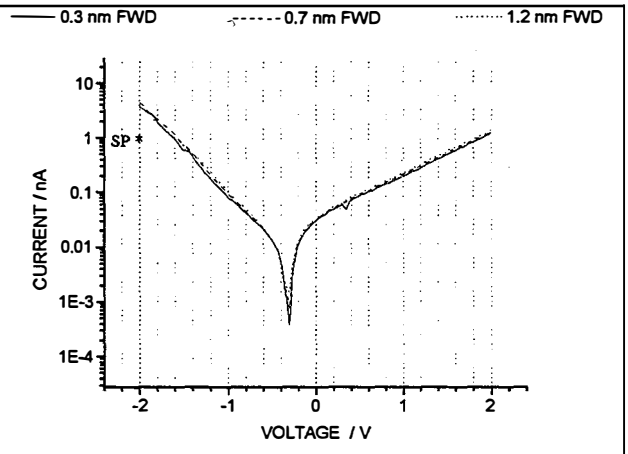

Fig. 5b
The I-V characteristics change clearly at the intrinsic a-Si:H layer of the top cell. The strong asymmetry and the low conductivity, which does not increase although the tip was moved even further than on the ZnO/Al layer, show that contact is made and a Schottky barrier determines the tunnel current.

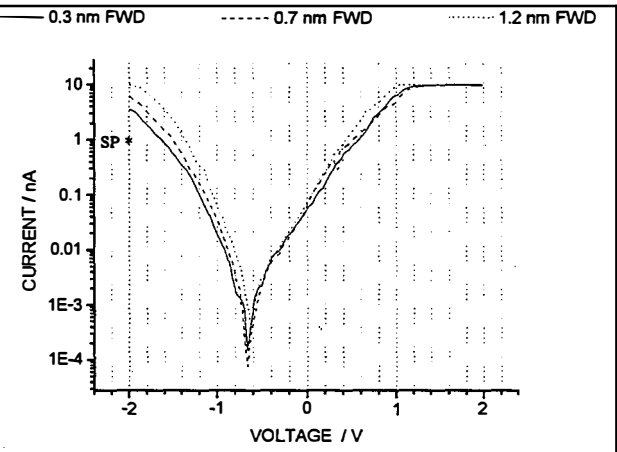

Fig. 5c In the region of the n-p junction the conductivity increases again and shows a more symmetric behavior. This can be observed in a wider range than the actual thickness of the two layers (10 nm each), while V_a undergoes large changes this region.

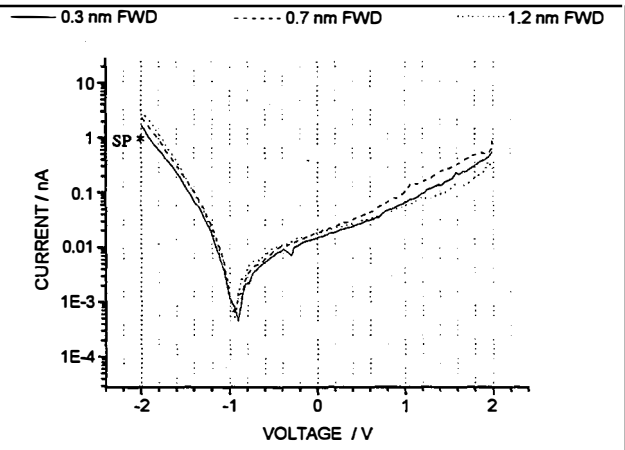

Fig. 5d On the intrinsic layer of the bottom cell the current changes back to asymmetric with low conductivity. The apparent potential moves further towards the induced voltage.

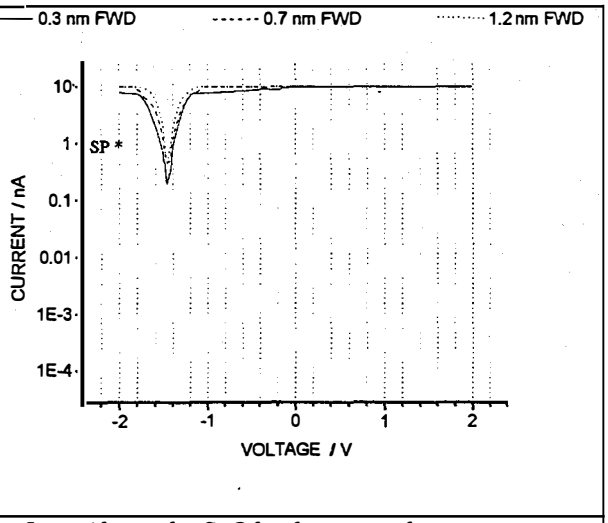

Fig. 5e Above the SnO back contact the characteristics again change dramatically. Very high conductivity and symmetry are observed. The apparent potential is exactly the voltage of 1.48 measured across the two contacts.

Fig. 5a-e STM spectroscopy across the cleaved and illuminated Solarex tandem cell.

We use a related voltage-feedback method of I-V measurement at controlled positions to establish the voltage (V_a) that yields zero current at each location. Here the current-distance feedback is turned off, the tip is moved forward (usually 0.5 –1.2 nm) in order to increase the sensitivity and a feedback is applied to the top contact voltage V_t, with the other contact open or fixed relative to V_t (see Fig.2). The feedback searches for the value where no tunnel current between the tip and the local surface flows. This is under computer control repeated as the tip scans across the cell. In **Fig.6** we show V_a (left axis) versus position (x) across the NREL cell, with no illumination but with forward and reverse bias of +/- 600 mV. A topographic scan (right axis) is also shown. V_a is measured at approximately 10 nm intervals for each scan; the positions of the interface between the intrinsic layer and the electrodes are indicated. The drop in V_a on the metal contact, to the left of x=0, occurs between the contact and the cleaved end of the cell due to low conductivity of the Au-Pd layer, which was kept very thin (~5 nm) to avoid tearing during the cleave. The voltage step at the ITO interface (or this could be at the i-p layer interface) is quite reproducible, and interesting although it is too early to draw conclusions. This step is also seen when the cell is forward biased with illumination, but this data is not shown in **Fig.6**.

In the TCO and highly-doped layers V_a is the Fermi level. In the intrinsic regions which are out of equilibrium V_a is related to the chemical potential, and is between the quasi-Fermi levels. However, at this time we do not have a full theory that relates V_a to the filled and empty states at each location. When, at each position in the cell, the probe voltage is between the electron and hole quasi-Fermi levels, electron and hole tunneling currents are opposed and a balance can be expected at some intermediate probe voltage. Each current is proportional to the associated carrier density, with electrons dominant near the n layer and holes near the p layer. Thus, the apparent potential V_a changes continuously from the electron quasi-Fermi level in the n layer to the hole quasi-Fermi level in the p layer. The value of the V_a at each position is clearly sensitive to the local energy of the band edges, and the shape of the V_a versus x curve is closely related to the electric field distribution in the i layer and at the interfaces. However, the exact relationship is not yet established. We have started to model this relationship in collaboration with Richard Crandall, using AMPS to model the cells. The main problem is the lack of a

STM tunneling theory that can be verified on crystalline semiconductors.

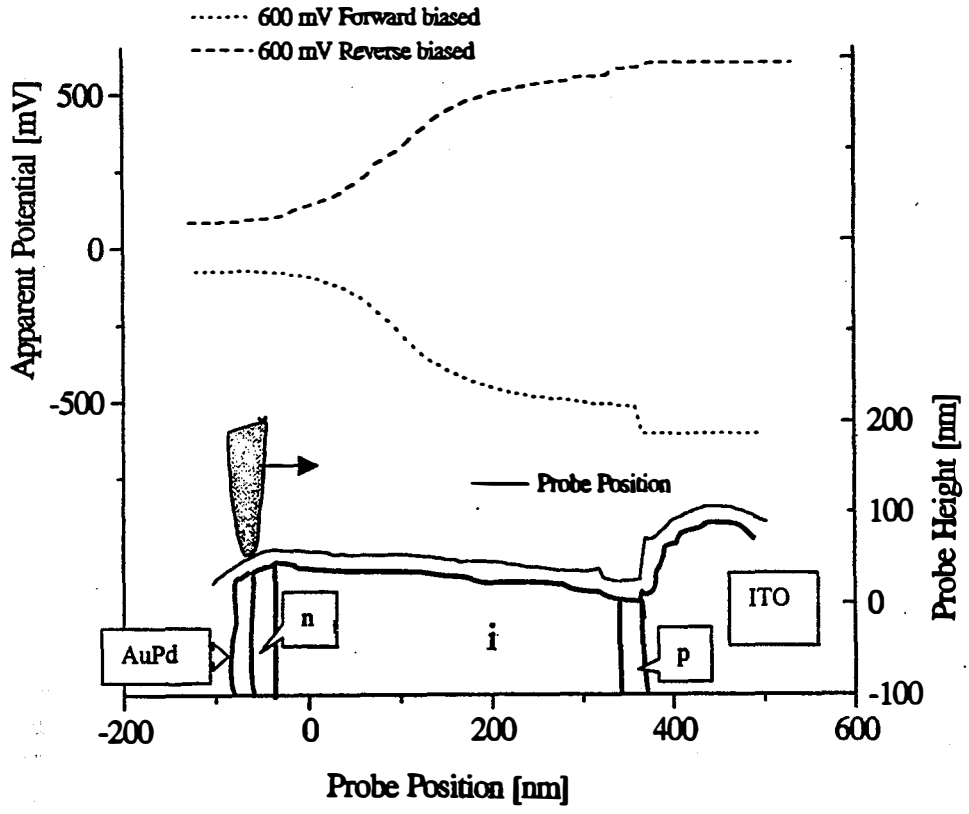

Fig 6 Diagrammatic representation of the 400 nm thick a-Si:H p-I-n cell on ITO from NREL and the probe. The measured topography of a linescan and the apparent potential for reverse and forward bias are shown.

Nonetheless, it appears that measurement of V_a versus position in the cell, when illuminated or biased, will provide considerable diagnostic power.

The I-V data can, in principle, be used to establish more than V_a at each position within the cell. A variety of publications in the STM literature suggest a relation between the I-V data and the semiconductor band edges and surface states, and as mentioned above we can discern clear differences between I-V curves on n and p layers of crystal Si. However, we do not yet find these theories very credible or useful, and we are attempting to advance the analysis to improve this situation. At the moment we have not yet diagnosed the entire I-V curves to see if they contain useful additional information. We have also not yet attempted to separate the a-Si:H n^+ and p^+ layers from the adjacent ITO and metal, although we plan to try using the low-voltage resistance.

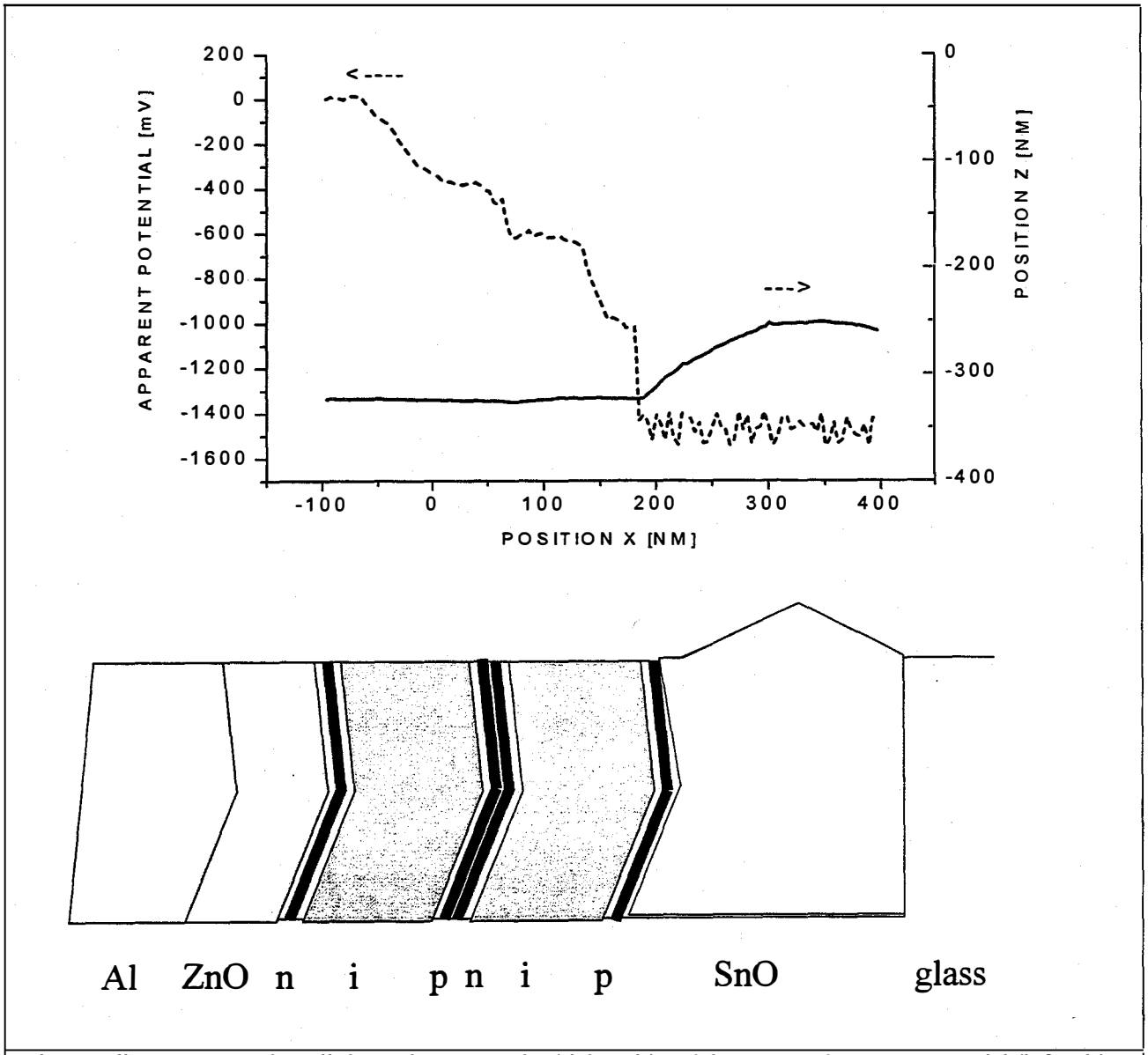

Fig.7 A linescan across the cell shows the topography (right axis) and the measured apparent potential (left axis), here on the Solarex tandem cell. Unfortunately, the results for V_a are not as reproducible as in the case of the single cell. At the bottom a schematic diagram shows the different layers.

In **Fig. 7** a linescan across the cell shows the topography (right axis) and the measured apparent potential (left axis), here on the Solarex tandem cell. Unfortunately, the results for V_a are not as reproducible as in the case of the single cell. The reason seems to be the low conductivity of the intrinsic films, a problem, which probably can be overcome by using the high gain amplifier which we have developed, but was not used during this sequence of measurements. The feedback, which determines the apparent potential, also needs further improvement. Problems with our present method arise from the large differences in the conductivity, and therefore the gain of the feedback loop. On the intrinsic layer it is too low to find the apparent potential precisely; on the high conducting SnO it oscillates as one sees in Fig 7.

Not all areas of the cleaved, exposed cell surface yield the same electrical properties. This is attributed to a variety of problems. Sometimes, it appears that the metal-film that forms one electrode has torn loose, and at other times a flap of metal appears to have folded over the cell surface. Next, we suspect that some regions of the cell surface are covered with loose debris from the cleave. This causes the probe to pick up material and loose its optimum tunneling properties. Finally, the cell surface sometimes has a lot of sloping regions, especially for the Solarex cells that are deposited onto deliberately rough, polycrystalline TCO to enhance light trapping. An example of this topology is shown in **Fig. 8**.

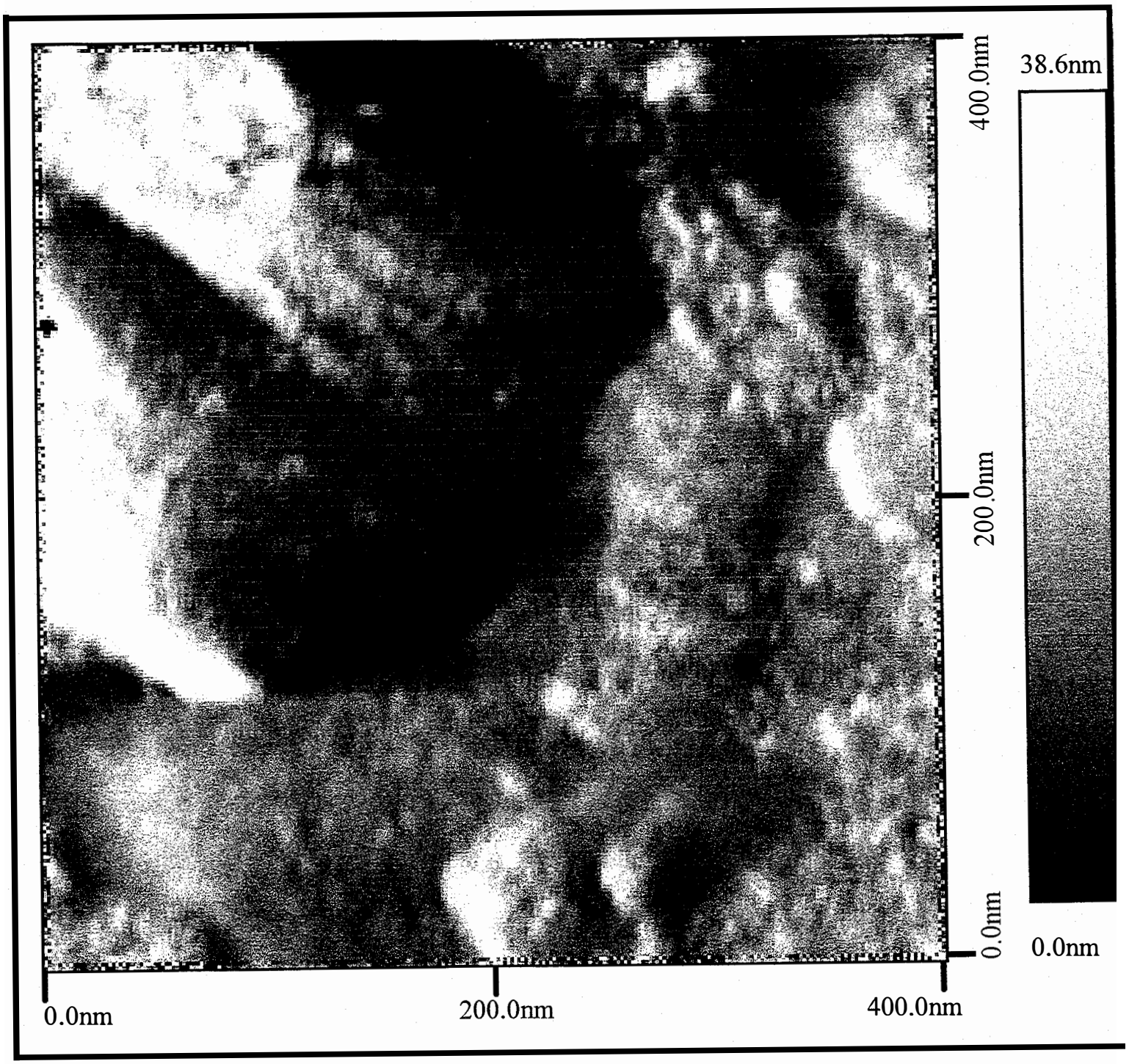

Fig. 8. A 400x 400 nm scan of the cleaved surface of the Solarex tandem cell.
Three interesting features are visible and can be identified with spectroscopy. On almost the entire right side one sees the SnO back contact, a rough film with individual hills. On the left side, visible only at the lower left quarter, one sees the relatively flat a-Si:H films where a change in the apparent voltage occurs. The big hill at the upper left is likely to be debris, either from the cleave or dragged around the corner by the tip during the approach. Fortunately, such features are not seen often.

Particle growth in silane rf discharges

Particle size and density are measured by light scattering techniques in a stainless steel electrode, capacitively coupled, rf silane discharge. The electrode gap (1.3 cm), gas pressure (0.2-0.5 Torr) and film deposition rate (1-8 Å/sec, related to rf power) mimic industrial cell deposition conditions. The discharge geometry is shown in Fig. 9. Of course, in this laboratory setup the electrode size (4x6 cm^2) is less than in industrial reactors, but we have preserved the character of width>>gap.

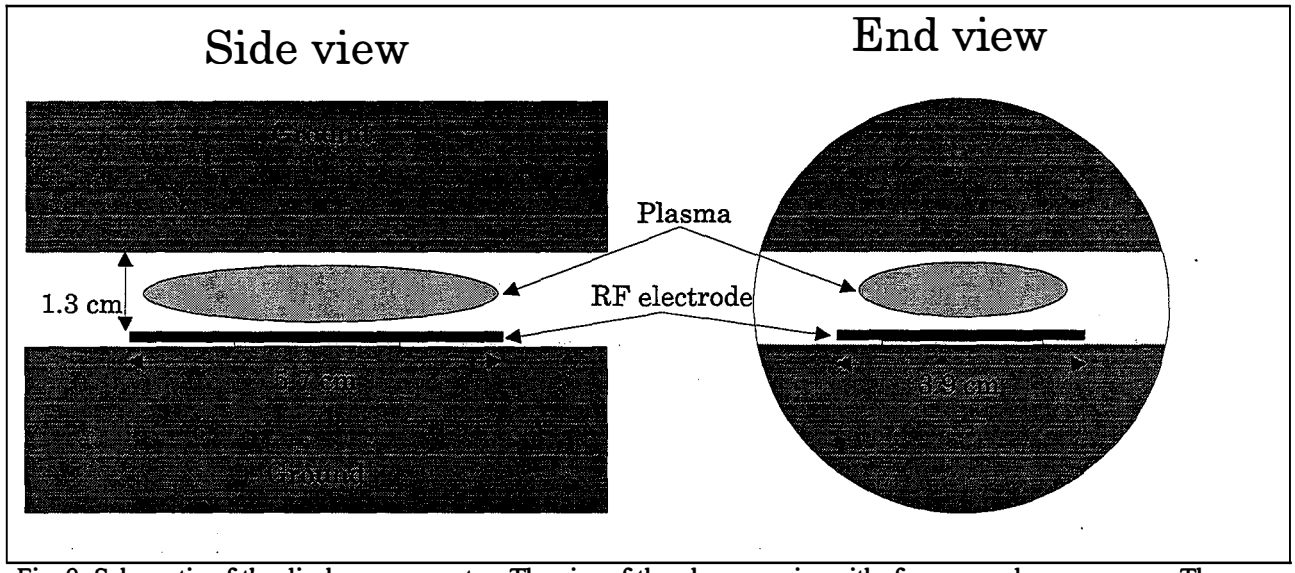

Fig. 9. Schematic of the discharge apparatus. The size of the plasma varies with rf power and gas pressure. The laser beam passes through the plasma parallel to the electrodes.

In order to simplify interpretation of measurements of small particle growth, the measurements reported here are performed without gas flow. Gas flow is a crucial element of a-Si:H deposition discharges and we previously measured particle scattering with gas flow. In our small-scale reactor the gas flow of ~1.5 sccm/cm^2 was constrained to flow between the electrodes resulting in a plug-flow speed of ~50 cm/sec. Under these conditions, the gas dwell time of ~0.1 sec is much shorter than the dwell time in a large-scale reactor. Thus, in a large-scale reactor negative clusters have more time to grow into nanometer-sized particles. The static-gas data reported here allow us to more reliably model the flowing-gas situation present in large-scale reactors, by comparing different discharge times in our reactor with corresponding downstream distances in the large-scale reactor. Furthermore, gas flow causes a spatial segregation of particle size, complicating measurement of growth and density.

A remote spark initiates the discharge in fresh SiH_4 gas; the discharge is allowed to run for a period of time (0.1-20 sec) and then is turned off. The spark (~15 cm from the rf electrodes) is used to start the discharge to avoid an overvoltage that would modify particle growth. (The rf circuit voltage is not very reduced when the rf discharge begins.) We have observed in the past that too large of a spark can itself result in creation of particles, so care is used to make a small spark that does not influence the dust.

An Ar^+ laser beam passes through the discharge volume parallel to the electrodes and scatters off the ensemble of particles during and after the discharge. Light scattered perpendicular to the beam is collected and measured by a photomultiplier tube (PMT) as a function of time. A typical trace of the PMT signal versus time is shown in Fig. 10. The signal increases when the discharge is started due to

discharge glow, and then grows due to particle scattering as the particles' size increases. Once the discharge is turned off, the scattered light signal decreases as the particles diffuse out of the scattering volume.

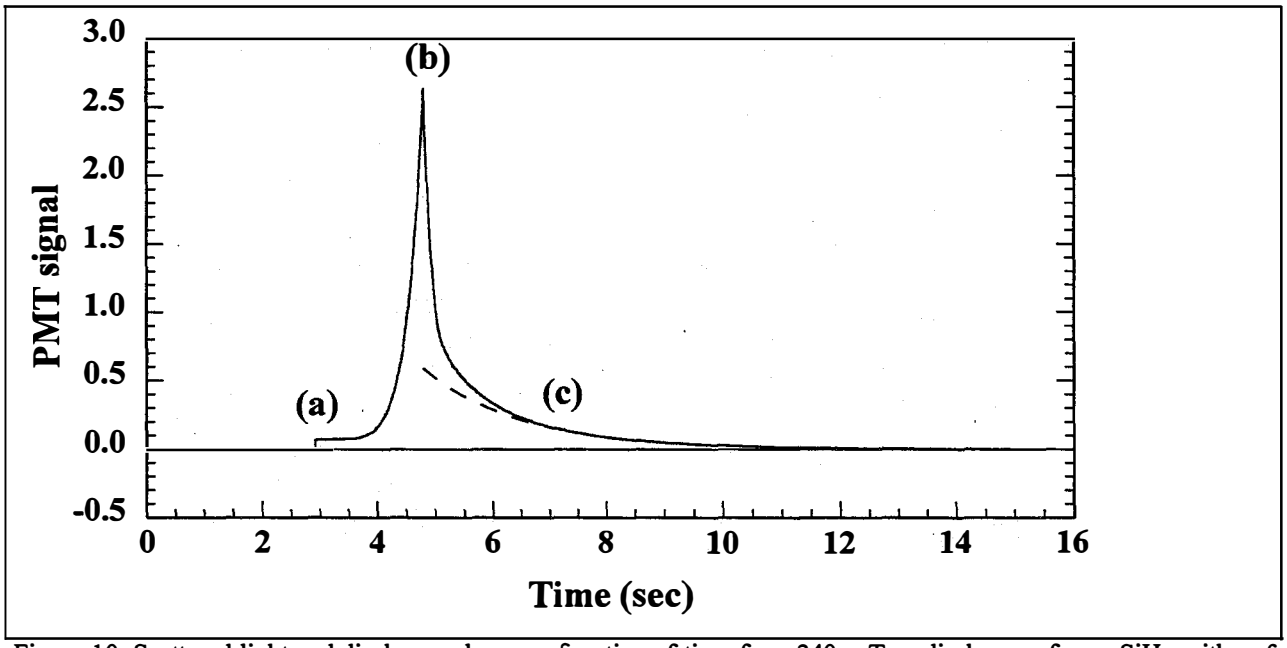

Figure 10. Scattered light and discharge glow as a function of time for a 340-mTorr discharge of pure SiH_4, with a rf voltage of 165 V peak-to-peak. At (a), the discharge is started. The scattered light signal builds until the discharge is switched off at (b). The scattered light in the late afterglow, beginning at (c), is fit to an exponential function (dashed line).

The particle size can be found from the rate of loss of the particles due to diffusion to the walls. The particles are negatively charged during the discharge, but they lose their charge in the afterglow by recombining with positive ions, so we model neutral diffusion. When the lateral extent of the particle cloud is larger than the electrode gap three-dimensional diffusion problem may be approximated by the one-dimensional diffusion equation. The solution of the ordinary diffusion problem in one dimension for a monodisperse size distribution is

$$n_p(z,t) = \sum_{m=1}^{\infty} a_m \sin\left(\frac{m\pi z}{h}\right) e^{-m^2 D \pi^2 t/h^2}$$

where h = electrode gap, D = particle diffusion coefficient, t is time after discharge termination, and the coefficients a_m are determined by the initial particle distribution. After an initial period in which the particle distribution adjusts into the fundamental mode shape, the complete solution reduces to a single exponential with a time constant of $h^2/D\pi^2$. Thus, the diffusion coefficient may be found from the decay rate, and the particle size is found from the diffusion coefficient, which is inversely proportional to the particle radius squared. [Hirschfelder, 1967]

Once the particle size is known from the rate of diffusive loss, the density of the particles can be found from the intensity of the scattered light. The scattering cross section of the particles is calculated as a function of r_p by assuming that their complex index of refraction is that of a-Si:H film. [Bohren, 1983] The scattered-light collection efficiency is calibrated from scattering by a gas with a known Rayleigh

cross section.

The above method of determining particle size and density is limited to situations in which the particle terminal velocity due to gravity or thermophoresis in the afterglow is small, and the residual charge on the particles in the afterglow is too small to result in ambipolar diffusion. We believe that these conditions are satisfied in the data reported here. If the size distribution is not monodisperse, only the largest particles are detected since the scattering cross section increases so rapidly with size ($\propto r_p^6$). Thus, at this stage we only report on the largest particles present.

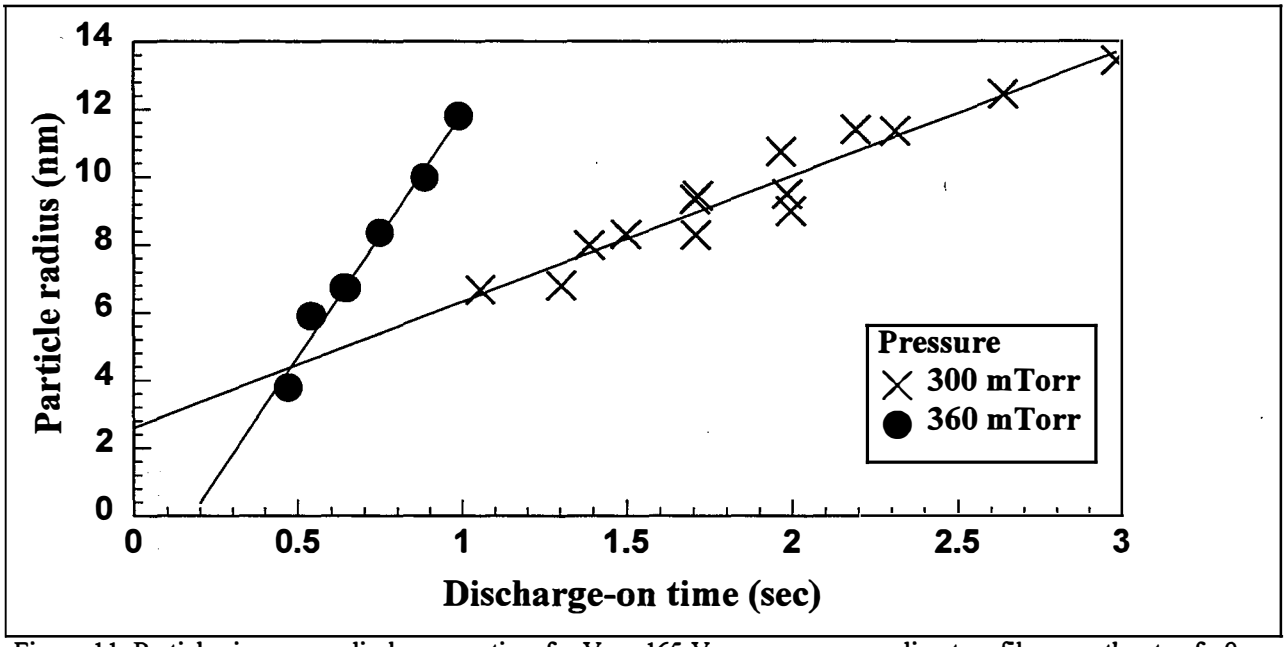

Figure 11. Particle size versus discharge-on time for V_{rf} = 165 $V_{peak\text{-}peak}$, corresponding to a film growth rate of ~9 Å/sec. Particle size is determined from the rate of loss of particles in the afterglow. The growth rate is found from the slope of the linear fit.

The particle size as a function of time that the discharge ran is shown in Fig. 11 for two different pressures. As can be seen, the particle size increases linearly with on time for both pressures. However, since these lines do not intersect with the origin and the particles must start with a radius of zero, he growth must be non-linear before the particles are large enough to be observed. The growth rates reported throughout this paper are from fits to the data that are not forced to go through the origin, as in Fig. 11. A linear growth rate of r_p implies that the rate at which material is incorporated into the particle is proportional to the area of the particle ($\propto r_p^2$). This follows from the fact that the number of atoms in the particle (N) is proportional to r_p^3, so $dN/dt \propto r_p^2\, dr_p/dt$. Since the growth due to the flux of positive ions is estimated to be much less than the observed growth rate, they can be ruled out as the primary particle growth species. Silane can also be eliminated as the primary growth species since the particle growth rate increases faster than the pressure. The remaining options for species resulting in particle growth are radicals such as SiH_3 or agglomeration with uncharged clusters.

Particle growth rate increases with pressure and with rf voltage, as shown in Fig. 12. Data is not shown below 280 mTorr, because the particle density is too low to detect the particles before they become so large that gravity becomes important, making determination of size difficult. Also, the scattering cross

section is no longer proportional to r_p^6, making determination of density more complex. The particle growth rates below 320 mTorr for a rf voltage of 165 $V_{peak-peak}$ and below 360 mTorr for 156 $V_{peak-peak}$ are consistent with growth due to SiH_3. The SiH_3 densities are determined by measuring the film growth rates with flowing gas. Since the film growth is primarily due to SiH_3, the film growth rate determines the radical density. However, the particle growth rate increases dramatically at higher pressures, to the point that SiH_3 can no longer account for all of the growth. Perhaps this additional growth is due to agglomeration with small, uncharged particles, but there is not yet direct evidence to support this hypothesis. While at higher pressures an additional process becomes important, growth due to SiH_3 radicals certainly continues.

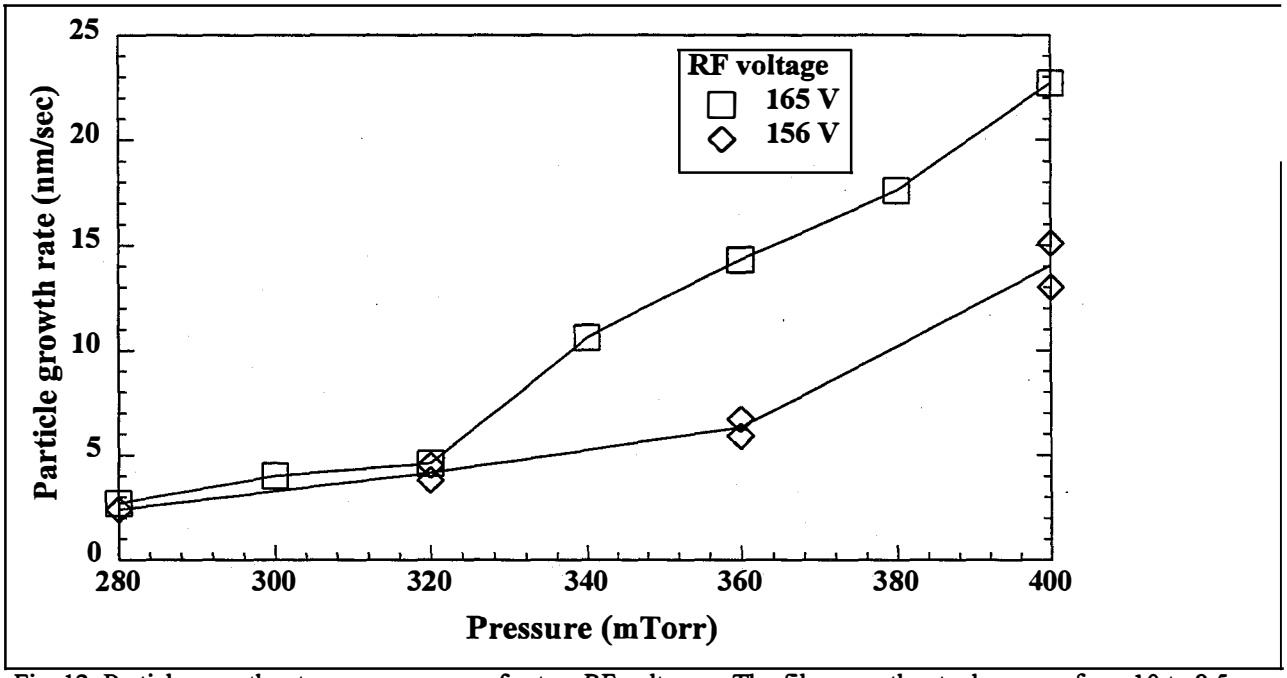

Fig. 12. Particle growth rate versus pressure for two RF voltages. The film growth rate decreases from 10 to 8.5 Å/sec for V_{rf} =165 V as the pressure increases from 280 to 400 mTorr; and, similarly, the film growth rate decreases from 9 to 7.5 Å/sec for V_{rf} = 156 V.

While the particle size increases with time, the particle density decreases as shown in Fig. 13. Here, the reported density is not the intensity corresponding to the peak signal when the discharge is switched off (point b in Fig. 10), but is instead the amplitude of the exponential fit at the time when the discharge is switched off (the initial value of the dashed line in Fig. 10). This method was selected because it is less sensitive to noise in the PMT signal and it is less sensitive to the initial particle distribution. The actual peak densities are 3-4 times the densities in the plot, because the initial distribution is more sharply peaked than the fundamental mode of the one-dimensional diffusion equation solution. The decrease in particle density as a function of time while the discharge is on is a conundrum: particles are normally expected to be charged negatively and held in the plasma by ambipolar electric fields. They are also prevented from agglomerating by Coulomb repulsion, and in any case even neutral-neutral agglomeration rates are too small to account for the observed density decrease. There is no evidence that the particle cloud changes position within the plasma, causing an apparent density decrease in the illuminated region. Thus, one is forced to conclude that particles are leaving the plasma. At present we have no detailed explanation of this observation, although it is consistent with our previous observations of particles incorporated into the a-Si:H film.

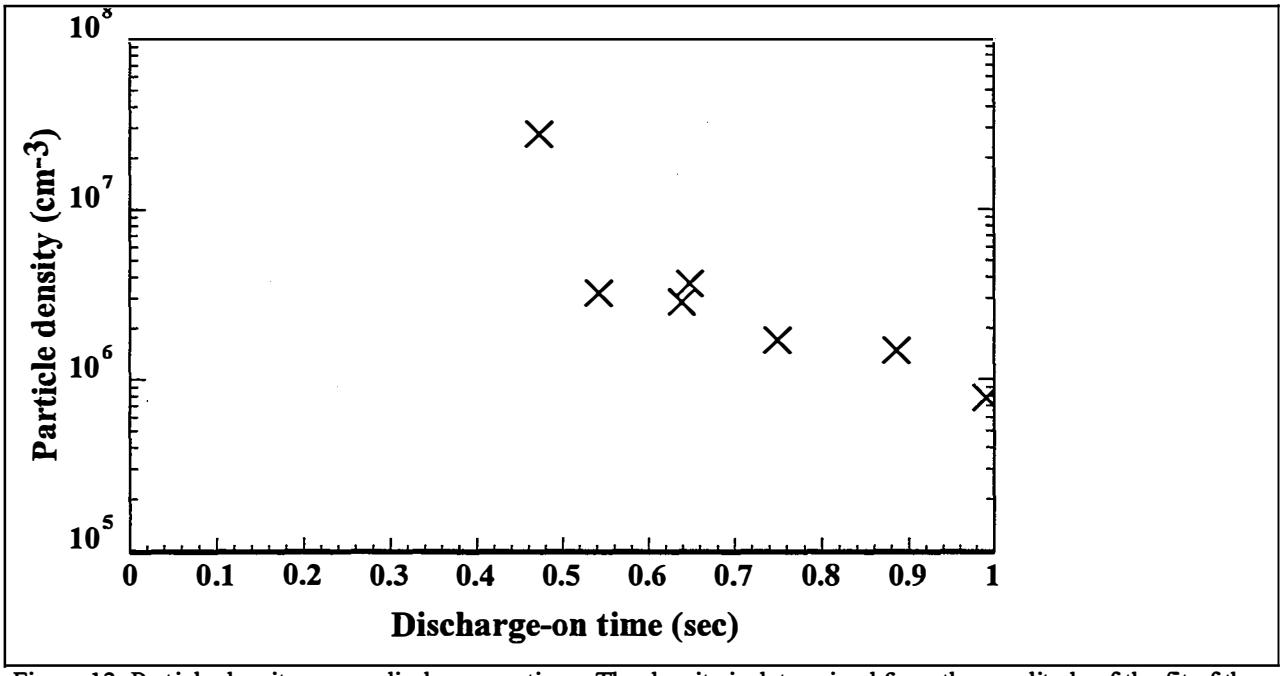

Figure 13. Particle density versus discharge-on time. The density is determined from the amplitude of the fit of the decaying scattered light signal in the afterglow and the particles' scattering cross section. For these data, V_{rf} is 165 V and the gas pressure is 360 mTorr.

In order to compare the particle densities under different pressures and rf voltages, the density when the particle radius is 8 nm is plotted in Fig. 14. This shows that the density increases rapidly with pressure and with rf voltage.

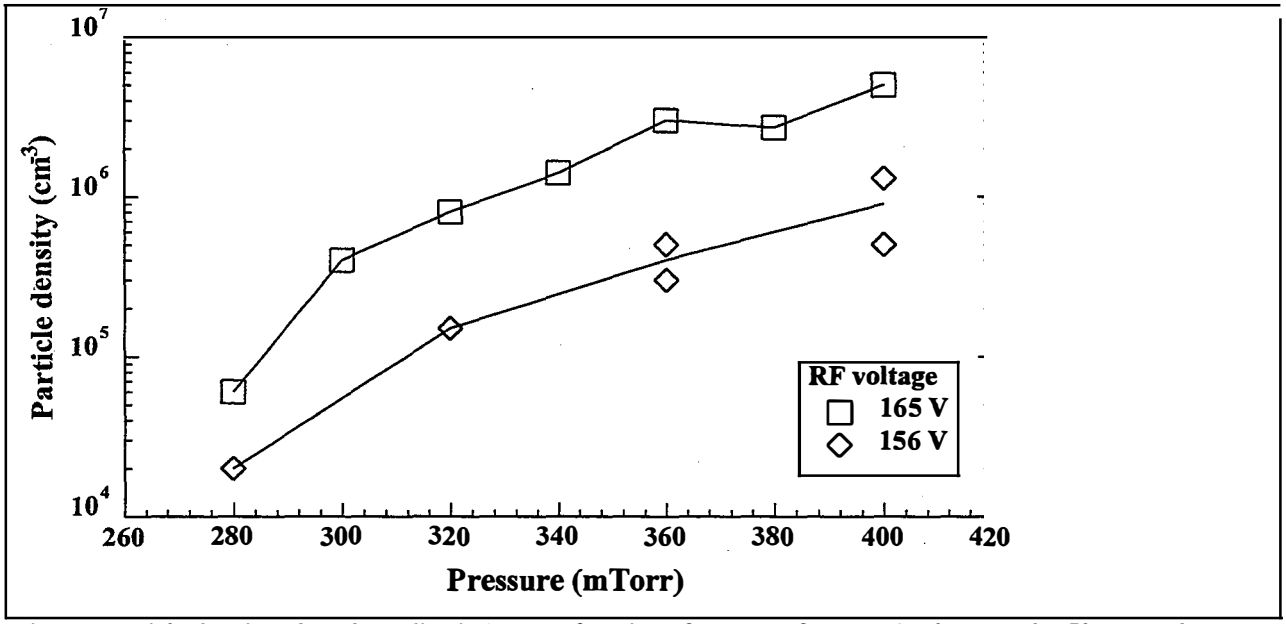

Fig. 14. Particle density when the radius is 8 nm as function of pressure for two rf voltages. The film growth rates differ by 10% at the two voltages.

Conclusions

Using a Scanning Tunneling Microscope (STM) we have developed a new method to investigate a-Si:H solar cells. The STM tunnels into different regions of a cross sectioned cell, to measure electronic properties through the cell. During this period a variety of technical problems were solved. The cells are cleaved in the UHV chamber and remain intact (minimal debris, no torn films, continuous voltage drop across the cell) at the cleaved surface. The tip is brought into tunneling with the cross section without being destroyed or picking up loose material. STM spectroscopy yields to reproducible data. The contact layers and the intrinsic a-Si:H can be identified, and the apparent potential can be measured. We still need to further refine and automate some aspects of the measurements, such as the measurement of resistance versus probe-sample gap. We also need to develop a more complete theory of the apparent potential versus position within the cell. However, it is clear that these STM observations can provide an interesting new method for diagnosing PV cell properties and light-induced degradation. We look forward to soon diagnosing cells from other a-Si:H Team laboratories.

A new technique for measuring particle sizes has been developed and applied to silane rf a-Si:H deposition plasmas. This allows measurement of 4-30 nm radius particles, which overlaps the size range (1-8 nm) of particles that have been detected in a-Si:H films. In this technique, the particle size is determined from the particle loss rate in the afterglow due to diffusion. The particle density is then found from the intensity of the scattered light using the particle size. Our main results are (1) that the particle growth rate is linear after a brief period of non-linear growth, (2) that the particle density decreases during the discharge, and (3) that most particle growth in this size range is due to attaching Si atoms from SiH_3. The growth rate at lower pressures is consistent with SiH_3 only, but additional growth due to an as-yet-unidentified species occurs at higher pressures. The second result, in conjunction with previous observations of particles in the film using a STM, strongly suggests that particles continually leave the plasma and are incorporated into the film. Future work involves further investigation of the growth of particles in the gas phase. In particular, the initial non-linear growth period will be examined and the strong dependence of particle density and growth rate on pressure and rf voltage will continue to be studied. The effect of increased gas temperature on particle growth also will be studied. Furthermore, application of amelioration techniques such as thermophoresis, electrode shaping, or chopping the discharge to control particle incorporation in the film will be tested.

References

Bohren, C.F., Huffman, D.R.; Absorption and Scattering of Light by Small Particles (Wiley, New York, 1983), p. 132.

Gallagher, A.; Tanenbaum, D.; Laracuente, A.; Jalencovic,B (July 1995). *Atomic-ScaleCharacterization of Hydrogenated Amorphous-Silicon Films and Devices, Final Subcontract Report, 15 April,1994—14 April 1995.* NREL/TP-411-8246. Golden, CO: National Renewable Energy Laboratory.

Gallagher, A.; Barzen, S.; Childs, M.; Laracuente, A.; (Feb 1997). *Atomic-ScaleCharacterization of Hydrogenated Amorphous-Silicon Films and Devices, Final Subcontract Report, 14 February,1995—14 April 1996.* NREL/SR-520-22565. Golden, CO: National Renewable Energy Laboratory.

Hirschfelder, J.O.; Curtiss, C.F.; Bird, R.B.; Molecular Theory of Gases and Liquids (Wiley, New York, 1967), p. 14. In the limit that the particle is much larger than a gas molefule, the diffusion coefficient according to the rigid-sphere model is

$$\mathbf{D} = 2.628 \times 10^{-3} \frac{\sqrt{\mathbf{T}^3 / 2\mathbf{M}}}{\mathbf{p}\sigma / 2}, \mathrm{cm}^2/\mathrm{sec}$$

where **M** = gas molecular weight, **T** = temperature in K, **p** = pressure in atm and σ = particle diameter in Å.

Schmidt, U.I.; Schröder, B.; Oechsner, H. (11 December 1993). "Influence of Powder Formation in a Silane Discharge on a-Si:H Film Growth Monitored by *In Situ* Ellipsometry." J.Non-Cryst. Sol. 164-166, 127 (1993)

Smith, A.R.; Chao, K.-J.; Shih, C.K.; Shih, Y.C., Streetman, B.G. (23 January 1995). "Cross-Sectional Scanning Tunneling Microscopy Study of GaAs/AlAs Short Period Superlattices: The Influence of Growth Interrupt on the Interfacial Structure." Appl. Phys. Lett. (66:4); pp. 478-480.

Tanenbaum, D.M.; Laracuente, A.; Gallagher, A.; Matr. Res. Soc. Symp. Proc. 377, 143 (1995).

Tanenbaum, D.M.; Laracuente, A.; Gallagher, A.; Appl. Phys. Lett. 68, 1705 (1996).

REPORT DOCUMENTATION PAGE

Form Approved
OMB NO. 0704-0188

1. AGENCY USE ONLY (Leave blank)	2. REPORT DATE	3. REPORT TYPE AND DATES COVERED
	June 1998	Annual Subcontract Report; 15 April 1994 – 14 March 1998

4. TITLE AND SUBTITLE
Atomic-Scale Characterization of Hydrogenated Amorphous-Silicon Films and Devices; Annual Subcontract Report, 15 April 1994 – 14 March 1998

5. FUNDING NUMBERS
C: DAD-4-14084-01
TA: PV804401

6. AUTHOR(S)
A. Gallagher, S. Barzen, M. Childs, and A. Laracuente

7. PERFORMING ORGANIZATION NAME(S) AND ADDRESS(ES)
National Institute of Standards and Technology
University of Colorado
JILA
Boulder, CO 80309-0440

8. PERFORMING ORGANIZATION REPORT NUMBER

9. SPONSORING/MONITORING AGENCY NAME(S) AND ADDRESS(ES)
National Renewable Energy Laboratory
1617 Cole Blvd.
Golden, CO 80401-3393

10. SPONSORING/MONITORING AGENCY REPORT NUMBER
SR-520-24760

11. SUPPLEMENTARY NOTES
NREL Technical Monitor: B. von Roedern

12a. DISTRIBUTION/AVAILABILITY STATEMENT

12b. DISTRIBUTION CODE
UC-1262

13. ABSTRACT *(Maximum 200 words)*

The research is concerned with improving the electronic properties of hydrogenated amorphous silicon (a-Si:H) films and of photovoltaic (PV) cells that use these films. Two approaches toward this goal are being taken. One is to establish the character of silicon particle growth in the rf glow discharges that are used to make the films and PV cells, and to understand the particle incorporation into the films. The ultimate goal of this effort is to find mitigation techniques that minimize the particle incorporation. During this contract period, we developed a novel particle light-scattering technique that provides a detailed and sensitive diagnostic of small (8-60-nm diameter) particles suspended in the discharge. We used this to measure the particle growth rates and densities, versus conditions in pure-silane discharges. The second program is directed toward measuring the electronic properties of thin-film PV cells, as a function of depth within the cell. The approach being taken is to use a scanning tunneling microscope (STM) to measure the depth-dependent electronic properties of cross-sectioned PV cells. During the present period, measurements on single and tandem amorphous silicon cells have been carried out. Using STM current-voltage spectroscopy, these measurements distinguish the boundaries between the highly conducting and intrinsic layers, and should allow one to deduce the chemical potential versus depth in the cell.

14. SUBJECT TERMS
photovoltaics ; hydrogenated amorphous silicon ; a-Si:H films ; atomic-scale characterization ; scanning tunneling microscopy ; films and devices

15. NUMBER OF PAGES
27

16. PRICE CODE

17. SECURITY CLASSIFICATION OF REPORT	18. SECURITY CLASSIFICATION OF THIS PAGE	19. SECURITY CLASSIFICATION OF ABSTRACT	20. LIMITATION OF ABSTRACT
Unclassified	Unclassified	Unclassified	UL